SCIENTIFIC REPORTS

OPEN

Thermal Transport in Fullerene Derivatives Using Molecular Dynamics Simulations

Liang Chen[1], Xiaojia Wang[2] & Satish Kumar[3]

In order to study the effects of alkyl chain on the thermal properties of fullerene derivatives, we perform molecular dynamics (MD) simulations to predict the thermal conductivity of fullerene (C_{60}) and its derivative phenyl-C61-butyric acid methyl ester (PCBM). The results of non-equilibrium MD simulations show a length-dependent thermal conductivity for C_{60} but not for PCBM. The thermal conductivity of C_{60}, obtained from the linear extrapolation of inverse conductivity vs. inverse length curve, is 0.2 W m^{-1} K^{-1} at room temperature, while the thermal conductivity of PCBM saturates at ~0.075 W m^{-1} K^{-1} around 20 nm. The different length-dependence behavior of thermal conductivity indicates that the long-wavelength and low-frequency phonons have large contribution to the thermal conduction in C_{60}. The decrease in thermal conductivity of fullerene derivatives can be attributed to the reduction in group velocities, the decrease of the frequency range of acoustic phonons, and the strong scattering of low-frequency phonons with the alkyl chains due to the significant mismatch of vibrational density of states in low frequency regime between buckyball and alkyl chains in PCBM.

Fullerene and its derivatives have gained enormous attention for the application in low-cost, flexible organic photovoltaic devices[1–3] due to the strong absorption coefficients for ultraviolet and visible light, as the major spectrum of solar radiation[4,5] and relatively higher electron mobility[6] than other polymers. Besides, owing to the ultra-low thermal conductivity, fullerene and its derivatives have also been studied as advanced thermoelectric materials[7] and thermal insulation materials for phase change memory devices[8]. A good understanding of the thermal transport mechanism and length dependent thermal properties of fullerene and its derivatives are important in order to accurately consider the effect of Joule heating and heat losses in these devices.

There have been a few experimental studies on the thermal conductivity of fullerene and its derivatives. Thermal conductivity of single crystal C_{60} was first measured using static one-heater, two-thermometer method, and the reported values are around 0.4 W m^{-1} K^{-1} which is nearly temperature independent above 260 K[9,10]. Later, 3ω method was used to characterize the thermal conductivity of a C_{60}/C_{70} compact, which was shown to be 0.1 W m^{-1} K^{-1} at room temperature[11]. Recently, fullerene derivatives were found to have ultra-low thermal conductivity, which is even lower than that of C_{60} solids. Duda *et al.*[12,13] measured thermal conductivity of phenyl-C61-butyric acid methyl ester (PCBM) using time-domain thermoreflectance (TDTR), and reported exceptionally low values around 0.03 ~ 0.06 W m^{-1} K^{-1} at room temperature. Wang *et al.*[14] conducted TDTR measurements to study the thermal conductivity of fullerene C_{60} and its derivatives including PCBM and phenyl-C61-butyric acid n-buylester (PCBNB). They observed low thermal conductivity of PCBM and PCBNB around 0.05 ~ 0.06 W m^{-1} K^{-1}. In addition, they found the thermal conductivity of disordered C_{60} was about 0.1 W m^{-1} K^{-1} at room temperature, nearly a factor of two larger than that of PCBM or PCBNB. As noted by both groups, the conventional

[1]School of Energy and Power Engineering, Xi'an Jiaotong University, Xi'an, P.R. China. [2]Department of Mechanical Engineering, University of Minnesota, Minneapolis, United States. [3]G. W. Woodruff School of Mechanical Engineering, Georgia Institute of Technology, Atlanta, United States. Correspondence and requests for materials should be addressed to X.W. (email: wang4940@umn.edu) or S.K. (email: satish.kumar@me.gatech.edu)

minimum thermal conductivity model[15] fails to explain the ultralow thermal conductivity of fullerene derivatives by counting the exact atomic number density in a unit cell. Considering two extremes of pure fullerene (disorder C_{60} films)[11,14] and pure organic alkyl-chain systems (amorphous polymers)[16,17], both have higher thermal conductivities than the fullerene derivatives. Therefore, fullerene derivatives such as PCBM and PCBNB cannot be simply treated as a mixture of fullerene and alkyl chains in the study of their thermal conductivity, and their thermal transport mechanisms are complicated by adding the alkyl chains to buckyballs via chemical bonding. Besides, the unusual reduction of thermal conductivity was also observed in the measurements[18] of the intercalated polymer-PCBM composite. The results showed a lower thermal conductivity of the composite than both of the constituents when the polymer volumetric fraction is below 35%, and similar mechanism was suggested for the reduction of thermal conductivity.

The role of alkyl chains in the thermal transport of fullerene derivatives and their effects on the phonon properties remain unclear. Based on the measurements of picosecond acoustics, both Duda et al.[13] and Wang et al.[14] discovered that the longitudinal speed of sound is ~20%–30% lower in PCBM or PCBNB than that in C_{60}. It has been speculated that the alkyl chains attached to buckyballs affect the low frequency phonons, leading to reduction in the speed of sound as well as the thermal conductivity of fullerene. Further study is required for better understanding of the thermal transport mechanisms in fullerene and its derivatives, which is important to engineer their thermal properties with molecular modification and explore the lower limit of thermal conductivity of fully dense solids.

In this work, we study the thermal transport in crystalline C_{60} and its derivative PCBM using molecular dynamics (MD) simulations. We first perform equilibrium MD simulations to obtain the vibrational density of states (VDOS) of crystalline C_{60}, disordered C_{60}, and crystalline PCBM. We find the mismatch of VDOS in the low frequency regime between buckyballs and alkyl chains in PCBM can lead to strong phonon scattering. We also observe a strong peak near zero frequency in the VDOS of crystalline C_{60} and disordered C_{60} at 300 K, corresponding to the rotation of single buckyball molecule which is totally suppressed in PCBM. Next, we calculate the thermal conductivities of C_{60} and PCBM of different domain lengths (~7 nm to 33 nm) at room temperature using non-equilibrium MD (NEMD) simulations. We observe strong size effects on the thermal conductivity of C_{60}. The extrapolated thermal conductivity of C_{60} is 0.2 W m^{-1} K^{-1}, which is a factor of 2 larger than that of PCBM (saturates at 0.075 W m^{-1} K^{-1} beyond 20 nm). Based on the different length dependence of the thermal conductivities of C_{60} and PCBM and the reduction in the speed of sound of PCBM observed by the aforementioned works, we attribute the decrease in the thermal conductivity of PCBM to the scattering of low frequency phonons imposed by alkyl chains.

Results and Discussion

In MD simulations, the face-centered cubic (FCC) C_{60}[19–21] and simple hexagonal (HEX) PCBM[13,22–25] are used at room temperature as shown in Fig. 1[43]. The phase transition of C_{60} from simple cubic to FCC occurs at a temperature of 250 K ~ 260 K[19]. But PCBM and other fullerene derivatives have quite different phase behavior due to the pendant groups of alkyl chains attached to C_{60} buckyballs[24–26]. As the annealing temperature increases, PCBM undergoes both amorphous-to-crystalline and crystalline-to-crystalline phase transformations which involve hexagonal crystals and needlelike crystals[24,25]. Since previous TDTR measurements indicate that the differences in the thermal conductivities of disordered and microcrystal-line PCBM are negligible, so we use HEX lattice for PCBM crystal in the MD simulations.

Phonon Dispersions of C_{60} and PCBM.

The phonon dispersions of FCC C_{60} crystal and PCBM with HEX lattice are obtained using harmonic lattice dynamics calculations with the inter-atomic force constants (IFCs) determined from frozen phonon method[27]. The primitive unit cell with one molecule is used for both FCC C_{60} and HEX PCBM. The interactions within a $5 \times 5 \times 5$ supercell and a $4 \times 4 \times 4$ supercell are included in the calculation of IFCs for FCC C_{60} and HEX PCBM, respectively. The molecular structures are relaxed in individual lattices using a conjugate gradient energy minimization algorithm at zero temperature. Figure 2 depicts the phonon dispersion curves of FCC C_{60} in its entire frequency range from 0 ~ 225 meV. In order to better elucidate the dispersion features, the frequency range is split into three frequency regimes corresponding to the three columns of Fig. 2. Since the primitive unit cell of 60 carbon atoms is used for the FCC C_{60} crystal, there are 180 branches of dispersion curves. As shown in the first column of Fig. 2, a large gap is observed between the intermolecular phonon branches (below 6.4 meV) and intramolecular phonon branches (above 30 meV). The 174 branches above 30 meV, as illustrated in Fig. 2, correspond to intra-molecular vibrations between bonded carbon atoms, which have negligible contributions to thermal transport due to their small group velocities.

According to the rigid-molecule approximation[28], the buckyball in FCC lattice can be treated as a rigid unit with point mass, and its motion is controlled by the net force and the net torque each of which has three degrees of freedom. In our calculations of the FCC C_{60} crystal, there is only one buckyball in each primitive unit cell. Thus there are six branches of dispersion curves below 8 meV, as illustrated in Fig. 3(a), which correspond to intermolecular motions including three translation components and three libration components[21]. In low-frequency regime below 8 meV, three acoustic branches are observed with larger group velocities which characterize the translational vibrations of buckyballs. The other three branches with small group velocity are observed below 1.5 meV which represent the librational
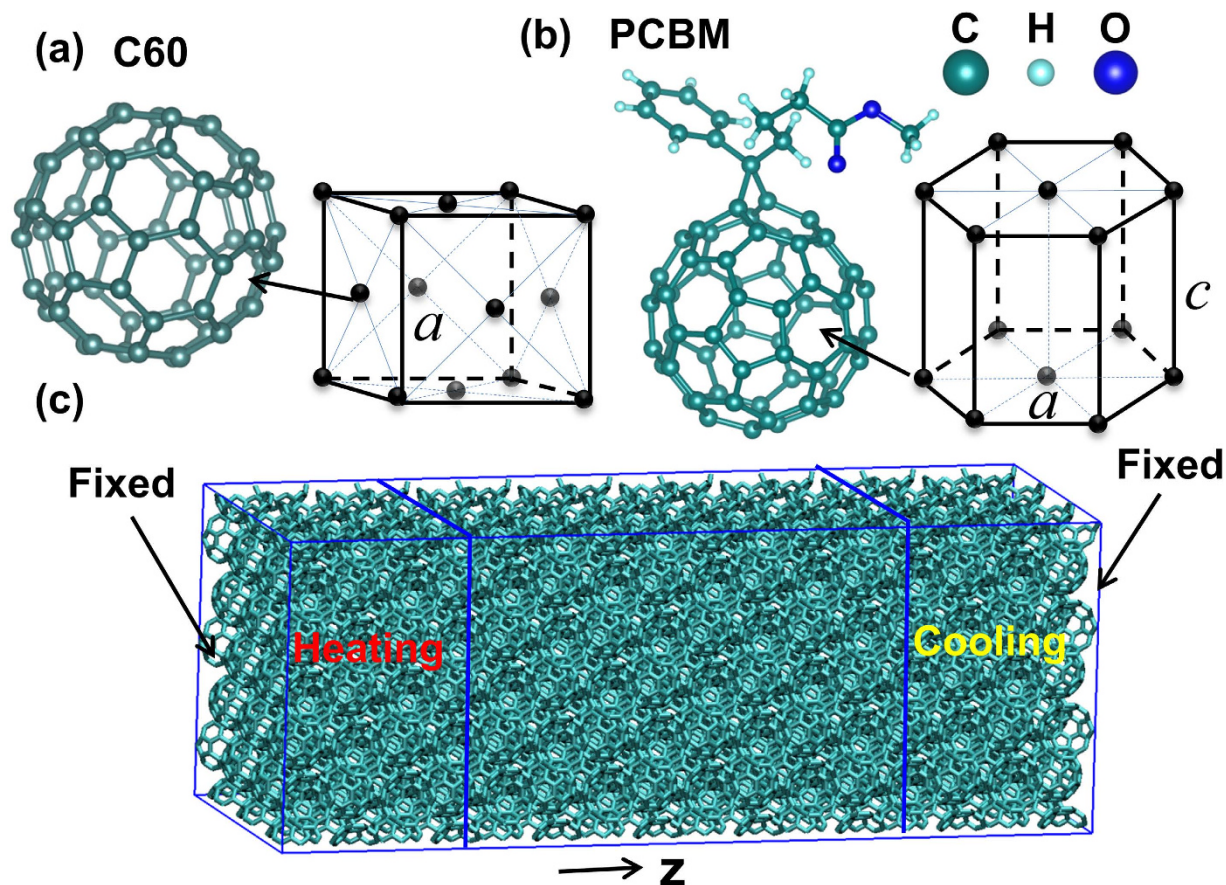
Figure 1. Molecular structures of (**a**) C_{60} and (**b**) PCBM. (**c**) Schematic diagram of system used in NEMD simulations. The system of C_{60} has face-centered-cubic lattice structure with lattice constant of $a = 13.98\,\text{Å}$. The PCBM has simple hexagonal lattice with lattice constants of $a = 10.1\,\text{Å}$ and $c = 10.4\,\text{Å}$. Figure drawn by L Chen using VESTA 3.2.1 for the molecular structure.
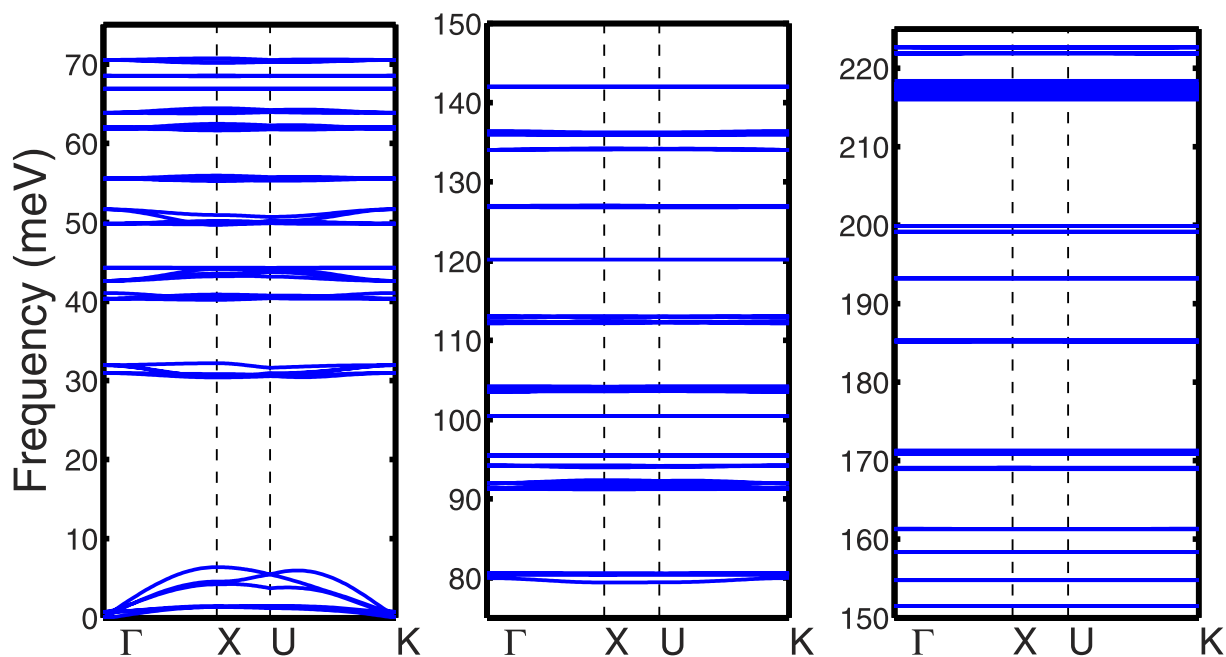

Figure 2. Lattice dynamics calculations of phonon dispersion curves of FCC C_{60}. The dispersion curves are divided into three columns of different phonon frequencies for better visualization.
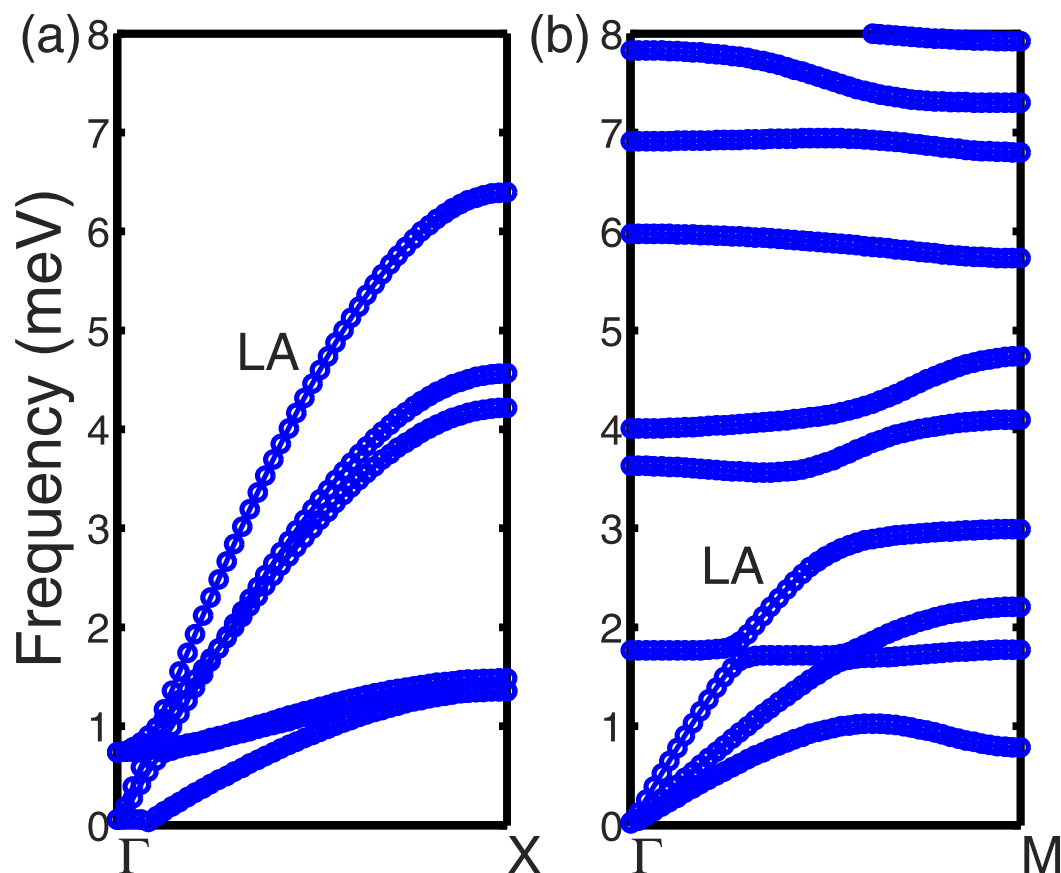
Figure 3. Phonon dispersions at frequency below 8 meV for (**a**) FCC C_{60} and (**b**) simple-hexagonal PCBM.

vibrations. Here, the librational vibration means the molecules rotate slightly back and forth with a nearly fixed orientation, as restricted by external forces or constraints.

The comparison of dispersion curves between C_{60} and PCBM is shown in Fig. 3 for frequency below 8 meV. It is observed that the maximum frequency of acoustic branches is reduced from 6.4 THz in C_{60} to 3.0 THz in PCBM, which indicates that fullerene is stiffer than its derivatives with alkyl chains. Above the acoustic branches in PCBM, optical branches are observed with small separations. The absence of the band gap in PCMB phonon dispersion between intermolecular modes and intramolecular modes allows more scattering of the low-frequency intermolecular phonons, and thereby lower their phonon mean free path and subsequently the thermal conductivity.

In Fig. 4, the phonon group velocities as a function of frequency are plotted for FCC C_{60} and HEX PCBM, based on the phonon dispersions determined from LD calculations. The first Brillouin zone (FBZ) is sampled with a $21 \times 21 \times 21$ q-point grid for both FCC C_{60} and HEX PCBM. Figure 4 shows the magnitude of group velocities at the irreducible q-points in the FBZ, e.g., 450 points for FCC C_{60} and 4630 points for HEX PCBM, respectively. The maximum group velocities, corresponding to the longitudinal acoustic branches near Γ point, are ~3.6 km s^{-1} for both FCC C_{60} and HEX PCBM. It can be observed in Fig. 3 that the group velocity (or the slope) of the longitudinal branch in FCC C_{60} remains similar along the Γ-X line, while the group velocity of longitudinal branch in HEX PCBM starts to decrease to zero with the mid-points along the Γ-M line. Moreover, Fig. 4 shows the group velocity in C_{60} has a large population above 1 km s^{-1} while the majority population has group velocities lower than 1 km s^{-1} in PCBM. Therefore, the characteristic group velocity should be lower in PCBM than C_{60}. The group velocities shown in Fig. 4 are consistent with the measurement results in literature[12–14], which has reported the longitudinal speed of sound is ~3.3 ~ 3.8 km s^{-1} in C_{60} and decreases by 20% to 30% in PCBM. It has been suggested that the lower speed of sound in PCBM may be one of the reasons responsible for the reduction in its thermal conductivity compared to C_{60}[12–14,18].

Comparing the Vibrational Density of States. In order to explore the effects of alkyl chains on phonon states in C_{60} and PCBM, we calculate the VDOS which describes the frequency-dependent distribution of phonon modes. Figure 5(a) plots the VDOS of FCC C_{60} and the buckyball of HEX PCBM at 300 K. In C_{60} or PCBM, the phonon modes with frequency above ~7 meV correspond to the intra-molecular vibrations dominated by the C-C bonding[21]. In Fig. 5(b), a peak centered at 0.35 meV
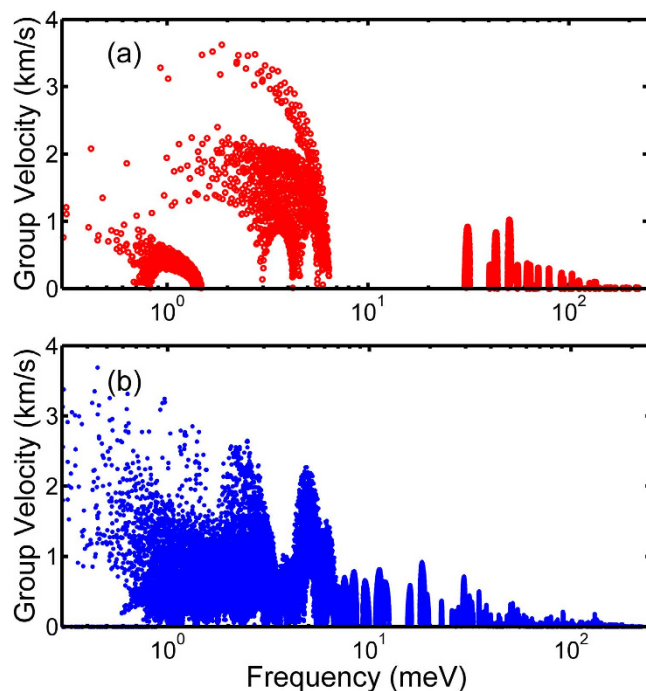
Figure 4. Phonon group velocity as a function of frequency for (**a**) FCC C_{60} and (**b**) simple-hexagonal PCBM.
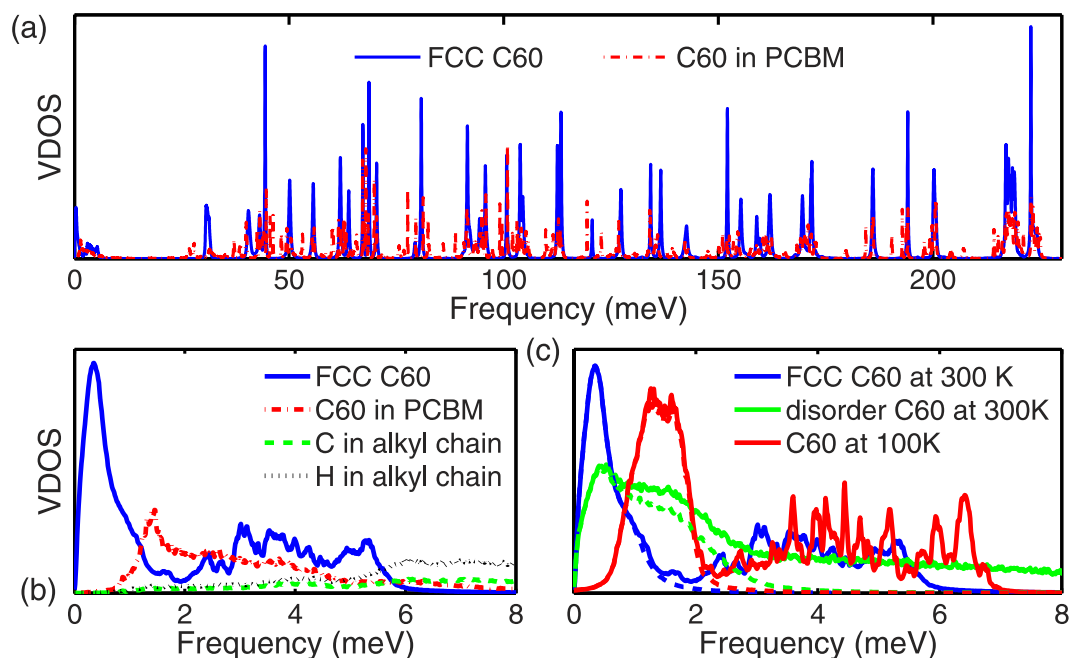

Figure 5. (**a**) VDOS of FCC C_{60}, and carbon atoms in simple hexagonal PCBM at 300 K; (**b**) Magnified low-frequency regime of VDOS in Fig. 5(a); also shown in Fig. 5(b) are the VDOS of C and H atoms in the alkyl chain of PCMB. (**c**) Low-frequency regime of VDOS of FCC C_{60} at 100 K and 300 K and disordered C_{60} at 300 K. The dashed lines (partly overlapped with solid lines) indicate the VDOS with translational momentum balanced for each C_{60} molecule.

is observed for the VDOS of FCC C_{60} at room temperature, which is also found in previous MD simulations[29]. However, the large population of phonon modes around 0.35 meV is not observed in the dispersion curves shown in Fig. 3(a). The discrepancy is caused by the rotational motion of C_{60} molecules at room temperature. The optimization of C_{60} structure and LD calculations are performed at the

temperature of zero Kelvin, and all buckyballs in the supercell have the same orientation as the one in the primitive unit cell. However, the buckyballs of the C_{60} supercell in MD are allowed to rotate; hence the orientation of buckyball can change once the energy barrier between different local minima of energy surface is overcome[30]. At room temperature, the energy barriers to overcome for changing buckyball orientation are negligible compared to their kinetic energy; thus the buckyballs are nearly free to rotate[31]. We speculate that buckyballs in MD simulations undergo continuous diffusive rotational motions[32] with various orientations, leading to the diminished librational modes.

Neglecting the energy barriers caused by the intermolecular interactions, the isolated buckyball can be treated as the spherical top[32], a 3D rotator in which all three orthogonal rotations have equal inertia and they are highly symmetric. The DOS of a spherical top has a dependence on the square root of the frequency[33], which agrees well with the trend of VDOS at near zero frequency for FCC C_{60} at 300 K. Therefore the large VDOS at near zero frequency in C_{60} shall be attributed to the rotational motion of buckyballs. While in PCBM, the VDOS for buckyballs is nearly zero below 1 meV (see Fig. 3(b)) suggesting that the rotational motions are fully suppressed by the alkyl chains.

Compared with the VDOS of FCC C_{60}, above 10 meV, the peaks in the partial VDOS of the buckyballs in PCBM are shifted or new peaks are created because of the changes in intra-molecular bonding with the addition of alkyl chains. However, the VDOS of the buckyball in the low frequency regime, dominated by the inter-molecular interaction, have been modified significantly by the alkyl chains in PCBM, as depicted in Fig. 3(b). The VDOS of C and H atoms in alkyl chains of PCMB is also shown in Fig. 3(b). below 5 meV, the VDOS of C and H atoms in alkyl chain is small compared to that of the buckyballs in PCBM. This significant mismatch of VDOS between buckyballs and alkyl chains can cause intense scattering of low frequency phonons. As low frequency inter-molecular phonons may dominate the thermal transport in fullerene, the scattering by alkyl chains can lead to significant decrease of thermal conductivity.

In order to gain some insight on the phonon modes contributing the VDOS peak near zero frequency in C_{60}, we compare the VDOS of FCC C_{60} solid at 300 K and 100 K, and disordered C_{60} at 300 K in Fig. 3(c). Also shown in Fig. 3(c) are the VDOS plots (dashed lines) with translational momentum balanced for each C_{60} molecule. Here the translational momentum is balanced by removing the overall translational velocity components of a buckyball from the velocities of each atom in that buckyball[34]. It can be seen from Fig. 3(c), the removal of the translational momentum for each C_{60} molecule does not affect this low-frequency peak ($<$2 meV), but results in suppression of the VDOS beyond 2 meV. It should be noted that the similar phenomenon has been observed previously[19]. In disordered C_{60}, the VDOS peak near zero frequency is broadened to 4 meV, beyond which the VDOS diminishes to zero with the removal of translational momentum.

As the temperature reduces to 100 K, the rotation of buckyball is significantly hindered or even completely frozen near zero frequency for C_{60} at 100 K, as shown in Fig. 3(c). The peak of VDOS at around 1.5 meV for C_{60} at 100 K is not affected with the removal of the translational momentum. The suppression of VDOS at close-to zero frequencies ($<$0.5 meV) at 100 K can be attributed to the freezing of low frequency rotational motions of the buckyballs, as at low temperatures the kinetic energy is not high enough to overcome the energy barrier between local minima. The MD calculations of the VDOS agree well with the LD predictions for both the FCC C_{60} and the HEX PCBM at low temperatures.

To confirm our hypothesis on the correlation of the first low-frequency peak around 0.35 meV in the VDOS of C_{60} at 300 K and the buckyball rotational motion, we calculated the mean square displacement (MSD) which measures the spatial extent of random motion. In this work, the MSD is calculated in two ways: 1) the MSD of the mass center of the molecules, and 2) the MSD of atoms with the mass center translation removed. Figure 6 depicts the MSD as a function of time for C_{60} and PCBM. The MSD in Fig. 6 is normalized to its maximal value in the plotted range of time. It can be seen from Fig. 6(a) that the MSD of the mass center of molecules converges quickly to a small value ($\sim$0.14 Å^2) within 1 ps for both C_{60} and PCBM which indicated no drift of the structure during the simulation.

The MSD of the atoms with the mass center translation removed reflects the spatial extent of the rotational motion. As shown in Fig. 6(b), the profile of MSD of rotation in PCBM is similar to that of the MSD of molecule translation: it reaches the magnitude of 0.26 Å^2 within 1 ps and then fluctuates. However, the MSD of rotation in C_{60} is much higher ($\sim$23.6 Å^2), and it converges to the maximum value slowly. The profile of MSD versus time for C_{60} in Fig. 6(b) is fitted to a response function, $MSD = Ae^{-t/\tau} + B$. A time constant of 11 ps is obtained. This time constant gives a frequency of 0.37 meV which is in good agreement with the frequency ($\sim$0.35 meV) of the VDOS peak in Fig. 5(b) for C_{60} at 300 K. Therefore, the low frequency peak in VDOS for C_{60} at 300 K is attributed to the rotation of C_{60} molecules.

Thermal Conductivity Reduction in Fullerene Derivatives.

The thermal conductivities of FCC C_{60} and HEX PCBM are calculated using NEMD simulations[35]. In the NEMD simulations, size effects should be cautiously examined due to several reasons[36,37]: 1) the phonon mean free path may be larger than the system size; 2) long wavelength phonon modes are absent in the small system; 3) temperature jump at the boundary of heating/cooling bath. The NEMD predictions of thermal conductivity are shown in Fig. 7 for FCC C_{60} and HEX PCBM with different length along the z direction of the simulation
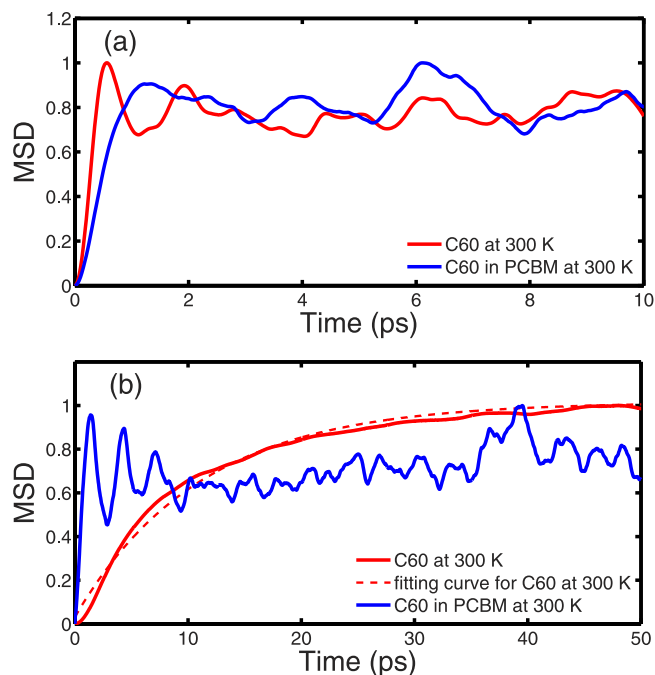
Figure 6. The normalized MSD as a function of time calculated for (**a**) mass center translations of molecules; (**b**) atom displacement after the mass center translation is removed. The MSDs are normalized to their maximum values during the period shown in the figure. The MSD of mass center of translation is $0.14\,\text{Å}^2$ for both C_{60} and PCBM at $300\,\text{K}$ in Fig. 6(a). MSD of rotation is $23.6\,\text{Å}^2$ for C_{60} and $0.26\,\text{Å}^2$ for PCBM at $300\,\text{K}$ in Fig. 6(b).
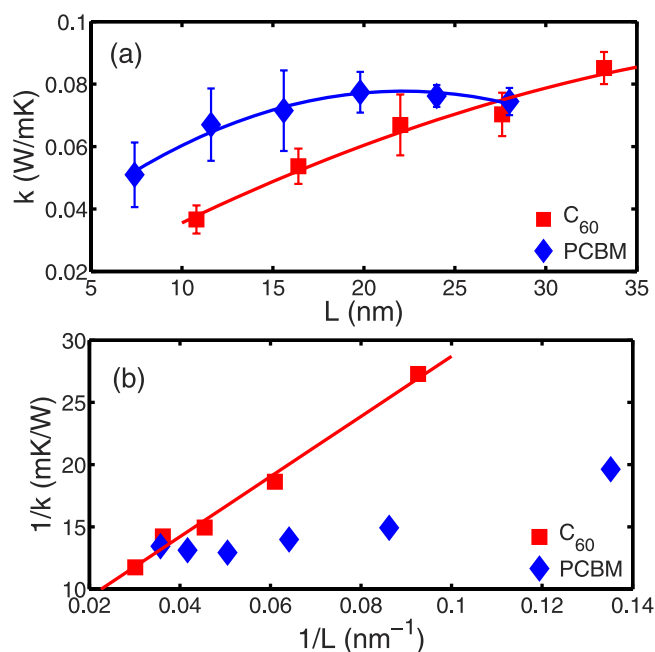

Figure 7. (**a**) Thermal conductivity of FCC C_{60} or simple hexagonal PCBM as a function of simulation domain size *L*. (**b**) Inverse of length-dependent thermal conductivity and the linear fitting of $1/k \sim 1/L$ for FCC C_{60}. The error bars in figure (**a**) denote the standard deviations calculated from MD samples.

domain. It can be observed that the thermal conductivity of FCC C_{60} increases as the length increased to $33\,\text{nm}$. But the thermal conductivity of PCBM saturates at $\sim0.075\,\text{W}\,\text{m}^{-1}\,\text{K}^{-1}$ beyond $20\,\text{nm}$. To compensate the contributions to the thermal conductivity of FCC C_{60} from phonons with mean free path

longer than 33 nm, we derive a linear relationship between $1/k$ and $1/L$ as shown in Fig. 4(b), and use the linearly extrapolated thermal conductivity of 0.2 W m^{-1} K^{-1} as the model prediction for FCC C$_{60}$.

Our NEMD predictions are smaller than the measured values of ~0.4 W m^{-1} K^{-1} around room temperature by Yu *et al.*[9] The discrepancy may be caused by the uncertainty in the measurements and the error in linear fitting in a relatively small range of system size considered in our NEMD simulations[36]. Besides, the difference in mass density of C$_{60}$ can also yield quite different thermal conductivity which has been already demonstrated in a previous study[38].

The predictions of FCC C$_{60}$ are larger than the previously reported thermal conductivity of ~0.1 W m^{-1} K^{-1} for highly disordered C$_{60}$ film from TDTR measurements by Wang *et al.*[14], and the C$_{60}$/C$_{70}$ compact from 3ω measurements by Olson *et al.*[11] This indicates the importance to include the factors limiting the phonon mean free path in the measured samples: 1) the C$_{60}$ molecules were highly disordered; 2) grain boundary presented; 3) impurities and defects could not be avoided. Our NEMD prediction of thermal conductivity of HEX PCBM is also higher than the measurements by Wang *et al.*[14] We attribute the discrepancy between the model prediction and the measured values for PCBM to the grain boundary, impurities, defects, the errors induced by the force field, and the uncertainties of the MD simulations.

Comparing the thermal conductivity predictions for FCC C$_{60}$ and PCBM, we observe a decrease of ~63%. This suggests the increased scattering by the alkyl chains for the dominant phonon modes in C$_{60}$. As shown in Fig. 2 for the phonon dispersion curves of FCC C$_{60}$, the high-frequency intra-molecular phonon modes are highly localized with very small group velocities; therefore, they contribute less to the thermal transport as compared with the low frequency inter-molecular phonons. Moreover, the comparison of VDOS shown in Fig. 5(b) also indicates strong scattering of low frequency phonons of buckyballs by the alkyl chains due to mismatch of phonon distribution. The low frequency phonons mostly consist of inter-molecular modes including both translational modes and librational modes. The individual contributions to thermal transport from the translational and librational modes are not yet determined. Further separation of the individual contributions to the suppression of the thermal conductivity of fullerene derivatives, from either librational or translational modes, requires a more detailed and systematic investigation of the mode-dependent phonon lifetime.

Conclusions

In summary, we have studied the VDOS and length-dependent thermal conductivity of crystalline C$_{60}$ and PCBM solids using MD simulations. We find there exists a significant mismatch of vibrational density of states in low frequency regime between buckyball and alkyl chains in PCBM. We also observe a larger phonon population with smaller group velocities at low frequencies in PCBM than C$_{60}$. Based on the NEMD predictions of length-dependent thermal conductivity, we obtain an extrapolated value of 0.2 W m^{-1} K^{-1} for FCC C$_{60}$ and a saturated value around 0.075 W m^{-1} K^{-1} for PCBM. The observed 62% reduction in the thermal conductivity from FCC C$_{60}$ to PCBM can be attributed to the reduction in group velocities and the frequencies of acoustic phonons, and the increased scattering of low frequency phonons by the alkyl chains due to mismatch of phonon spectrum.

Methods

Molecular Dynamics Simulation Parameters. We use Lammps package[39] for MD simulations and polymer consistent force field (PCFF) to describe the inter-atomic interactions including van der Waals, bonding, bond-bond angle, dihedral, and improper interactions[40,41]. The lattice constant of FCC C$_{60}$ is $a = 13.98$ Å which is determined by matching the measured mass density (1.75 g cm^{-3}) of C$_{60}$ samples[14]. For HEX PCBM, due to the difficulty in direct positioning of the PCBM molecule at each lattice site with optimized lattice constants, we first generate the initial structure with a large lattice constant, and then relax the system in isothermal-isobaric (NPT) ensembles. The optimized lattice constants of HEX PCBM are $a = 10.1$ Å and $c = 10.4$ Å, yielding a mass density of 1.65 g cm^{-3} which is within the range of density (1.4 ~ 1.8 g cm^{-3}) of PCBM samples in previous experiments[14,26]. For the calculation of VDOS, periodic boundary conditions are applied in all three Cartesian directions, and a supercell of 5.6 nm × 5.6 nm × 5.6 nm is used for C$_{60}$ while the domain size of PCBM is 5 nm × 5 nm × 5 nm. In the NEMD simulations, periodic boundary conditions are applied in the x and y directions while the two ends in the z direction are fixed as shown in Fig.1(c). A time step of 0.25 fs is used in all MD simulations.

Non-equilibrium Molecular Dynamics Simulations. A heating bath and a cooling bath are applied at left end and right end of the system, respectively. The heating/cooling bath is 3 nm long with ~4500 atoms. The constant heat transfer rate $\dot{q}$ at $+/-2$ nW is maintained in heating/cooling bath by rescaling the velocities of atoms. In order to reach the steady state, we first perform NEMD simulations for 5 ns before sampling. Then we sample the temperature along the z direction every 1.25 ns for another 12.5 ns. According to Fourier's law, the thermal conductivity is calculated as $k = \dot{q}/(A \cdot dT/dx)$, where A and dT/dx are cross-section area and temperature gradient in heat flux direction. The linear fitting of temperature profiles and calculation of thermal conductivity are performed every 1.25 ns. The reported thermal conductivity is the average of 10 samples for the period of 12.5 ns.

Vibrational Density of States and Mean Square Displacement. The VDOS $g(\omega)$ is calculated from the sampling of atom velocities in equilibrium MD simulations at room temperature[42]:

$$g(\omega) = \frac{1}{3N_a}\sum_{j}^{N_a}\sum_{\alpha}^{3}\left|\int v_{j,\alpha}(t)\,exp\,(-i\omega t)\,dt\right|^2 \tag{1}$$

where N_a is the number of atoms, and $v_{j,\alpha}$ is the velocity of atom j in direction α. The mean square displacement (MSD) of the mass center translation is given by

$$\text{MSD} = \left\langle \sum_{l}^{M}|\vec{r}_{c,l}(t) - \vec{r}_{c,l}(t_0)|^2 \right\rangle \tag{2}$$

where $\vec{r}_{c,l}$ is the position of the mass center of the molecule l, and the summation is over all the M molecules. The angled brackets denote an ensemble average. The MSD of atoms with the mass center translation is removed is given by

$$\text{MSD} = \left\langle \sum_{l}^{M}\sum_{j}^{N_0}\left|\left(\vec{r}_{j,l}(t) - \vec{r}_{c,l}(t)\right) - \left(\vec{r}_{j,l}(t_0) - \vec{r}_{c,l}(t_0)\right)\right|^2 \right\rangle \tag{3}$$

where $\vec{r}_{j,l}$ is the position of the atom j of molecule l, and the summation is performed over all the N_0 atoms in a molecule and then over all the M molecules. The positions and velocities are sampled every 20 steps for 2,000,000 steps. In PCBM, only the velocities of carbon atoms of the buckyball are sampled.

References

1. Blom, P. W. M., Mihailetchi, V. D., Koster, L. J. A. & Markov, D. E. Device physics of polymer: Fullerene bulk heterojunction solar cells. *Adv. Mater.* **19,** 1551–1566 (2007).
2. Li, G., Zhu, R. & Yang, Y. Polymer solar cells. *Nat. Photonics* **6,** 153–161 (2012).
3. Saran, R., Stolojan, V. & Curry, R. J. Ultrahigh performance C_{60} nanorod large area flexible photoconductor devices via ultralow organic and inorganic photodoping. *Sci. Rep.* **4,** 5041 (2014).
4. Sariciftci, N. S., Smilowitz, L., Heeger, A. J. & Wudl, F. Semiconducting polymers (as donors) and buckminsterfullerene (as acceptor) - photoinduced electron-transfer and heterojunction devices. *Synth. Met.* **59,** 333–352 (1993).
5. Sariciftci, N. S., Smilowitz, L., Heeger, A. J. & Wudl, F. Photoinduced electron-transfer from a conducting polymer to buckminsterfullerene. *Science* **258,** 1474–1476 (1992).
6. Singh, T. B. *et al.* Correlation of crystalline and structural properties of C_{60} thin films grown at various temperature with charge carrier mobility. *Appl. Phys. Lett.* **90,** 213512 (2007).
7. Zhang, K., Zhang, Y. & Wang, S. R. Enhancing thermoelectric properties of organic composites through hierarchical nanostructures. *Sci. Rep.* **3,** 3448 (2013).
8. Kim, C. *et al.* Fullerene thermal insulation for phase change memory. *Appl. Phys. Lett.* **92,** 013109 (2008).
9. Yu, R. C., Tea, N., Salamon, M. B., Lorents, D. & Malhotra, R. Thermal-conductivity of single-crystal C_{60}. *Phys. Rev. Lett.* **68,** 2050–2053 (1992).
10. Tea, N. H. *et al.* Thermal conductivity of C_{60} and C_{70} crystals. *Appl. Phys. A: Mater. Sci. Process.* **56,** 219–225 (1993).
11. Olson, J. R., Topp, K. A. & Pohl, R. O. Specific-heat and thermal-conductivity of solid fullerenes. *Science* **259,** 1145–1148 (1993).
12. Duda, J. C., Hopkins, P. E., Shen, Y. & Gupta, M. C. Thermal transport in organic semiconducting polymers. *Appl. Phys. Lett.* **102,** 251912 (2013).
13. Duda, J. C., Hopkins, P. E., Shen, Y. & Gupta, M. C. Exceptionally low thermal conductivities of films of the fullerene derivative PCBM. *Phys. Rev. Lett.* **110,** 015902 (2013).
14. Wang, X. J., Liman, C. D., Treat, N. D., Chabinyc, M. L. & Cahill, D. G. Ultralow thermal conductivity of fullerene derivatives. *Phys. Rev. B* **88,** 075310 (2013).
15. Cahill, D. G., Watson, S. K. & Pohl, R. O. Lower limit to the thermal-conductivity of disordered crystals. *Phys. Rev. B* **46,** 6131–6140 (1992).
16. Guo, Z. *et al.* Tuning the thermal conductivity of solar cell polymers through side chain engineering. *PCCP* **16,** 7764–7771 (2014).
17. Hu, C., Kiene, M. & Ho, P. S. Thermal conductivity and interfacial thermal resistance of polymeric low k films. *Appl. Phys. Lett.* **79,** 4121–4123 (2001).
18. Guo, Z. *et al.* Thermal conductivity of organic bulk heterojunction solar cells: An unusual binary mixing effect. *PCCP* **16,** 26359–26364 (2014).
19. Cheng, A. & Klein, M. L. Molecular-dynamics investigation of orientational freezing in solid C_{60}. *Phys. Rev. B* **45,** 1889–1895 (1992).
20. Gompf, F., Renker, B., Schober, H., Adelmann, P. & Heid, R. Inelastic neutron-scattering results on pure and doped fullerenes. *J. Supercond.* **7,** 643–645 (1994).
21. Yu, J., Kalia, R. K. & Vashishta, P. Phonon-dispersion and density-of-states of solid C_{60}. *Appl. Phys. Lett.* **63,** 3152–3154 (1993).
22. Cheung, D. L. & Troisi, A. Theoretical study of the organic photovoltaic electron acceptor PCBM: Morphology, electronic structure, and charge localization. *J. Phys. Chem. C* **114,** 20479–20488 (2010).
23. Napoles-Duarte, J. M., Reyes-Reyes, M., Ricardo-Chavez, J. L., Garibay-Alonso, R. & Lopez-Sandoval, R. Effect of packing on the cohesive and electronic properties of methanofullerene crystals. *Phys. Rev. B* **78,** 035425 (2008).
24. Zheng, L. D. & Han, Y. C. Solvated crystals based on [6,6]-phenyl-C_{61}-butyric acid methyl ester (PCBM) with the hexagonal structure and their phase transformation. *J. Phys. Chem. B* **116,** 1598–1604 (2012).
25. Zheng, L. D., Liu, J. G., Ding, Y. & Han, Y. C. Morphology evolution and structural transformation of solution-processed methanofullerene thin film under thermal annealing. *J. Phys. Chem. B* **115,** 8071–8077 (2011).
26. Choi, S. H., Liman, C. D., Kramer, S., Chabinyc, M. L. & Kramer, E. J. Crystalline polymorphs of [6,6]-phenyl-C_{61}-butyric acid n-butyl ester (PCBNB). *J. Phys. Chem. B* **116,** 13568–13574 (2012).

27. Togo, A., Oba, F. & Tanaka, I. First-principles calculations of the ferroelastic transition between rutile-type and CaCl$_2$-type SiO$_2$ at high pressures. *Phys. Rev. B* **78,** 134106 (2008).
28. Rafizade, Ha. & Yip, S. Lattice dynamics of hexamine - a rigid-molecule approximation. *J. Chem. Phys.* **53,** 315–325 (1970).
29. Cheng, A. L. & Klein, M. L. Molecular-dynamics simulations of solid buckminsterfullerenes. *J. Phys. Chem.* **95,** 6750–6751 (1991).
30. Liu, L. C. *et al.* Switching molecular orientation of individual fullerene at room temperature. *Sci. Rep.* **3,** 3062 (2013).
31. Sundqvist, B. Mapping intermolecular bonding in C$_{60}$. *Sci. Rep.* **4,** 6171 (2014).
32. Hollas, J. M. in Basic atomic and molecular spectroscopy (ed. Hollas, J. M.) 91–99 (The Royal Society of Chemistry, 2002).
33. Boudon, V. *et al.* in Handbook of high-resolution spectroscopy (eds. Quack, M. & Merkt, F.) 1437–1460 (John Wiley & Sons, Ltd, 2011).
34. Chen, L. & Kumar, S. Thermal transport in double-wall carbon nanotubes using heat pulse. *J. Appl. Phys.* **110,** 074305 (2011).
35. Chen, L., Huang, Z. & Kumar, S. Impact of bonding at multi-layer graphene/metal interfaces on thermal boundary conductance. *RSC Adv.* **4,** 35852–35861 (2014).
36. Sellan, D. P., Landry, E. S., Turney, J. E., McGaughey, A. J. H. & Amon, C. H. Size effects in molecular dynamics thermal conductivity predictions. *Phys. Rev. B* **81,** 214305 (2010).
37. McGaughey, A. J. H. & Kaviany, M. in Advances in heat transfer (eds. Greene, G. A., Cho, Y. I., Hartnett, J. P. & Bar-Cohen, A.) 169–255 (Elsevier, New York, 2006).
38. Andersson, O., Soldatov, A. & Sundqvist, B. Thermal conductivity of C$_{60}$ at pressures up to 1 GPa and temperatures in the 50-300 K range. *Phys. Rev. B* **54,** 3093–3100 (1996).
39. Plimpton, S. Fast parallel algorithms for short-range molecular-dynamics. *J. Comput. Phys.* **117,** 1–19 (1995).
40. Maple, J. R., Dinur, U. & Hagler, A. T. Derivation of force-fields for molecular mechanics and dynamics from abinitio energy surfaces. *Proc. Natl. Acad. Sci. USA* **85,** 5350–5354 (1988).
41. Sun, H. Ab-initio calculations and force-field development for computer-simulation of polysilanes. *Macromolecules* **28,** 701–712 (1995).
42. Chen, L. & Kumar, S. Heat dissipation mechanism at carbon nanotube junctions on silicon oxide substrate. *J. Heat Transfer: Trans. ASME* **136,** 052401 (2014).
43. Momma, K. & Izumi, F. VESTA 3 for three-dimensional visualization of crystal, volu-metric and morphology data. *J. Appl. Crystallogr* **44,** 1272–1276 (2011).

Acknowledgements

Author Contributions

X.W. conceived the idea. L.C. carried out the calculations and wrote the manuscript. Both X.W. and S.K. contributed to analyzing the data and revising the manuscript. All authors have reviewed and discussed the results and conclusions of this article.

Additional Information

Competing financial interests: The authors declare no competing financial interests.

How to cite this article: Chen, L. *et al.* Thermal Transport in Fullerene Derivatives Using Molecular Dynamics Simulations. *Sci. Rep.* **5**, 12763; doi: 10.1038/srep12763 (2015).